ARTICLE NO. 79-0152R

J80-090

Trailing Edge Conditions for Unsteady Flows at High Reduced Frequency

20009

Sanford Fleeter*
Purdue University, West Lafayette, Ind.

In the prediction of time-variant flows past isolated airfoils and airfoil cascades, the steady-state Kutta-Joukowsky condition is generally assumed to be valid. Recent experimental investigations on isolated airfoils however, have indicated that this assumption is only appropriate for flows characterized by low reduced frequency values. For the case of airfoil cascades, only low reduced frequency data exist, but these limited data indicate the same trend, i.e., the Kutta-Joukowsky condition is appropriate only for low reduced frequency values. Hence, the objective of the experimental investigation described herein was to determine the applicability of the Kutta-Joukowsky condition for isolated airfoils and airfoil cascades at high reduced frequency values over a range of incidence angles. This was accomplished by measuring the time-variant surface pressure distribution in the trailing edge region of a classical isolated flat plate, a classical flat plate cascade, and a cambered airfoil cascade, and correlating these data with an appropriate state-of-the-art zero incidence flat plate theoretical model that applies the Kutta-Joukowsky condition. The results obtained indicate that at these high reduced frequency values, the Kutta-Joukowsky condition is appropriate for the classical isolated flat plate and flat plate cascade over a wide range of incidence angles. However, for the cambered airfoil cascade, this condition does not appear to be satisfied for any value of incidence angle.

Nomenclature

b = airfoil semichord
C = airfoil chord
C_p = dynamic pressure coefficient, $\Delta P/(\rho \cdot V^2 \cdot v/V)$
C_p^* = individual surface dynamic pressure coefficient, $P/(\rho \cdot V^2 \cdot v/V)$
i = incidence angle
k = reduced frequency, $k = \omega b/V$
M = Mach number
V = absolute velocity
v = transverse perturbation velocity
ϕ = phase lag
ρ = inlet air density
ω = blade passing angular frequency

Introduction

THE steady-state Kutta-Joukowsky condition is generally applied in the prediction of the steady inviscid pressure distribution on both isolated airfoils and airfoils in cascade. This empirical requirement that the rear stagnation point be fixed avoids an infinite velocity in the flow around a sharp trailing edge. For the case of rounded trailing edges, the position of the rear stagnation point is indeterminate and must be determined from viscous considerations.

This problem is much more complex for time-variant flows[1,2] where the generally applied assumption for both isolated airfoils[3] and airfoils in cascade[4] is that no unsteady loading is permitted at the trailing edge. This assumption is in question, particularly for flows characterized by high reduced frequency values. Although unsteady loading variations in the trailing edge region of the airfoils may not significantly affect the magnitude of the unsteady lift, unsteady loading variations in the trailing edge region of the airfoils can significantly affect the unsteady moment. Also, aerodynamic phase lag variations in this region are particularly important with regard to noise generation. Hence, the proper theoretical modeling of the time-variant trailing edge condition for isolated airfoils and airfoils in cascade is an important consideration.

Several investigations involving controlled fluctuating flowfields past isolated airfoils and airfoils in cascade have been reported in the literature. For the case of isolated airfoils, the range of reduced frequency values investigated is relatively large, approximately from 0.05 to 5.0. For cascaded airfoils, however, data exist only for reduced frequency values to 0.08, a value well below that of interest for turbomachinery applications. However, these isolated airfoil and airfoil cascade data do indicate that the Kutta-Joukowsky condition may not be valid as the value of the reduced frequency increases and attains values of interest for design applications.

For an isolated uncambered airfoil, Satyanarayana and Davis[5] found that application of the Kutta-Joukowsky condition was appropriate for unsteady flows with reduced frequency values less than 0.6. For reduced frequency values greater than 0.8, the measured loading in the trailing edge region was larger than predicted, with this difference increasing with the reduced frequency. Commerford and Carta[6] investigated a circular arc airfoil at a reduced frequency value of 3.9 and concluded that the Kutta condition was satisfied. Their conclusion was based on the good correlation obtained between theory and the pressure differential magnitude data at the 90% chord location. However, the correlation of the theory with the pressure differential phase lag data in this trailing edge region was not nearly as good. Also, the correlation of the pressure differential magnitude data in the leading edge region of the airfoil was not very good, thereby casting some measure of doubt on the validity of the 90% chord pressure magnitude data-theory correlation and the subsequent conclusions concerning the Kutta condition. The pressure differential near the trailing edge of a flat plate and an airfoil at reduced frequency values greater than 5.0 were deduced by Archibald.[7] These results seem to indicate that the Kutta condition did not hold at this high reduced frequency value.

Presented as Paper 79-0152 at the AIAA 17th Aerospace Sciences Meeting, New Orleans, La., Jan. 15-17, 1979; submitted Feb. 28, 1979; revision received Aug. 13, 1979.

Index category: Nonsteady Aerodynamics.

*Associate Professor of Mechanical Engineering. Member AIAA.

For the case of airfoils in cascade, Ostdiek[8] measured the time-variant pressure distribution at reduced frequency values to 0.08. These results correlated well with theory over the leading edge region of the airfoils but not in the trailing edge region.

A most significant implication of the above experimental results is that the Kutta-Joukowsky condition may not be valid for flows characterized by reduced frequency values greater than unity for isolated airfoils or 0.1 for cascaded airfoils. This is of particular importance to turbomachinery applications wherein unsteady flows with first harmonic reduced frequency values to 10.0 and higher are encountered. Hence, the objective of the experimental investigation described herein is to determine the applicability of the Kutta-Joukowsky condition for isolated airfoils and airfoils in cascade at high reduced frequency values over a range of incidence angles. This is accomplished by measuring the time-variant pressure distribution in the trailing edge region of an isolated flat plate, a flat plate cascade, and a cascade of cambered airfoils, and correlating these unique data with an appropriate state-of-the-art flat plate theoretical model which applies the Kutta-Joukowsky condition.

Experimental Facility

The experiments described herein were conducted in the large-scale, low-speed, single-stage research compressor, schematically depicted in Fig. 1. This research compressor features 42 rotor blades that are aerodynamically loaded to levels typical of advanced multi-stage machines. Also, the rotor wake generated unsteady flow past the fixed airfoil stator row is characterized by a high first harmonic reduced frequency value, on the order of 8.0, which is of design interest to turbomachinery applications.

The rotor wake generated time-variant trailing edge pressures were measured in three separate fixed stator configurations: 1) a classical isolated flat plate; 2) a 40 vane classical flat plate stator row; and 3) a 40 vane cambered airfoil (NASA Series 65) stator row. A view of the rotor and the flat plate stator row is presented in Fig. 2. The mean section properties of all of the airfoils together with the compressor design point conditions are presented in Table 1.

The time-variant quantities of fundamental interest in this experimental investigation include the fluctuating aerodynamic forcing function—the rotor wakes, and the resulting trailing edge time-variant pressure distributions.

The airfoil surface dynamic pressure measurements were accomplished with flush mounted, Kulite, thin-line design dynamic pressure transducers. The trailing edge region of both surfaces of a single flat plate airfoil (92.0% and 96.0% of the chord) and one surface of each of two of the cambered airfoils (90.0% and 97.0% of the chord) were instrumented.

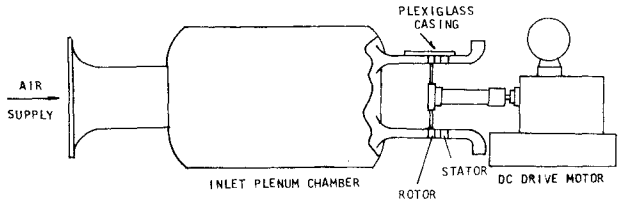

Fig. 1 Schematic of large-scale, low-speed, single-stage research compressor.

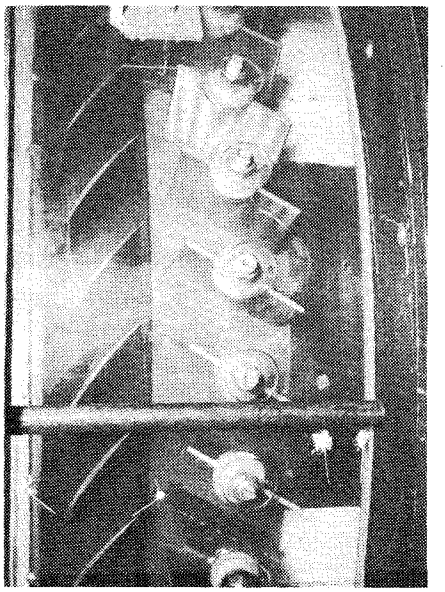

Fig. 2 View of rotor and flat plate stator row.

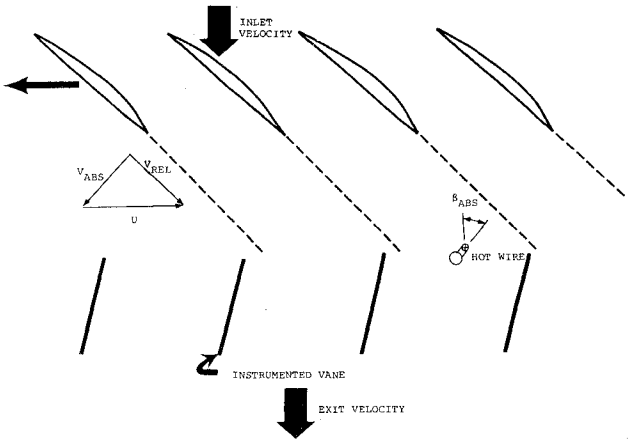

Fig. 3 Schematic of dynamic instrumentation.

Table 1 Airfoil mean section characteristics and compressor design point conditions

	Rotor	Flat plate stator	Cambered stator
Type of airfoil	65 series	Flat plate	65 series
Number	42	1,40	40
Chord C, cm (in.)	11.66 (4.589)	12.93 (5.089)	12.93 (5.089)
Solidity $\sigma = C/S$	1.435	1.516	1.516
Camber ϕ, deg	20.42	0.0	48.57
Aspect ratio $AR = S/C$	1.046	0.943	0.943
Loss coefficient	0.043	–	0.056
Diffusion factor	0.449	–	0.410
Flow rate, kg/s (lb/s)		14.07 (31.02)	
Tip speed, cm/s (ft/s)		5593.1 (183.5)	
Rotational speed, rpm		876.3	
Stage pressure ratio		1.0125	
Inlet tip diameter, cm (in.)		121.95 (48.01)	
Hub/tip radius ratio		0.80	
Stage efficiency, %		88.1	

The time-variant wake measurements were obtained by means of a cross-wire probe which was calibrated and linearized to 61.0 m/s and ±25 deg angular variation. The mean absolute exit flow angle from the rotor was determined by rotating the cross-wire probe until a zero voltage difference was obtained between the two linearized hot-wire signals. This mean angle was then used as a reference for calculating the instantaneous absolute and relative flow angles. The output from each channel was corrected for tangential cooling effects and the individual fluctuating velocity components parallel and normal to the mean flow angle calculated from the corrected quantities. The cross-wire probe was located axially immediately upstream of the leading edge of the stator row, as schematically depicted in Fig. 3.

Data Acquisition and Analysis

The time-variant data acquisition and analysis technique used is based on a data averaging or signal enhancement concept. The key to such a technique is the ability to sample data at a preset time. As the signal of interest is generated at the blade passing frequency, an optical encoder that delivers a square wave voltage signal having a duration of 1.5 μs was mounted on the rotor shaft. The computer analog-to-digital converter was triggered from the positive voltage at the leading edge of the pulse, thereby initiating the acquisition of the time unsteady data at a rate of up to 100,000 points/s. The data were sampled for N blade passages and over M rotor revolutions. These rotor revolutions were not consecutive because a finite time was required to operate on the N blade passage data before the computer returned to the pulse acceptance mode which initiated the gathering of the data.

Preliminary Fourier analysis of the wake data at the blade passage frequency indicated that the fifth harmonic had a content approximately 0.2 of that of the first harmonic (blade passage frequency). In order to accurately preserve the digitized signal, the number of points per cycle at the maximum rotor speed was set by operating the analog-to-digital converter on only two channels of data at its maximum rate of 100,000 points/s. For a blade passage frequency of 625 Hz, an A/D converter rate set at 100,000 points/s, and two channels of data, the resulting number of points acquired per cycle is 80.

A slight variation in wake profile existed from blade to blade, as determined by examining the averaged data for up to 12 rotor blade passages. At the reduced frequencies of these experiments, the vane surface was influenced primarily by three blade wakes. Hence, data were acquired for three blade passages. Also, it was found that the unsteady data were essentially unchanged when averaged for 100, 200, or 400 samples. Based on the above considerations, 80 to 100 digitized data points were obtained for each of three blade passages averaged over 400 rotor revolutions ($N=3$, $M=400$) in these experiments.

At each steady operating point an averaged time-variant data set, consisting of the two hot-wire and the Kulite transducer signals were obtained. The resulting digitized signals were then Fourier decomposed into harmonics. Figures 4 and 5 illustrate the Fourier analysis of the trailing edge dynamic pressure signal on the pressure surface of the cambered airfoil stator row. Figure 4 presents the averaged signal for three rotor blade passages for this transducer. Figure 5 presents only the center passage of the three seen in Fig. 4, showing the digitized data and the first three harmonics of the signal. Each of these harmonics has been summed with the zero term of the Fourier series. As seen, the sum of the first three harmonics yields a good approximation to the signal.

From the Fourier analysis of the time-variant data, both the magnitude and the phase angle as referenced to the data initiation pulse were obtained. The rotor exit velocity triangles were then examined to relate the rotor wake generated velocity profiles with the surface dynamic pressures on the instrumented vanes. Figure 6 shows the change in the rotor relative exit velocity which occurs as a result of the presence of the blade. A deficit in the velocity in this relative frame creates a change in the absolute velocity vector as indicated. This velocity change was measured via the crossed hot wires. From this instantaneous absolute angle and velocity, the rotor exit relative angle and velocity as well as the magnitude and phase of the perturbation quantities were determined.

As noted previously, the hot-wire probe was positioned immediately upstream of the leading edge of the stator row. To relate the time based events as measured by this hot-wire probe to the pressures on the vane surfaces, the assumptions were made that: 1) the wakes are identical at the hot wire and the stator leading edge planes and 2) the wakes are fixed in the relative frame. The rotor blade spacing, the vane spacing, and the axial spacing between the vane leading edge plane and the probe holder centerline are known quantities. With the above two assumptions, the wake was located relative to the hot wires and the leading edges of the instrumented vane suction

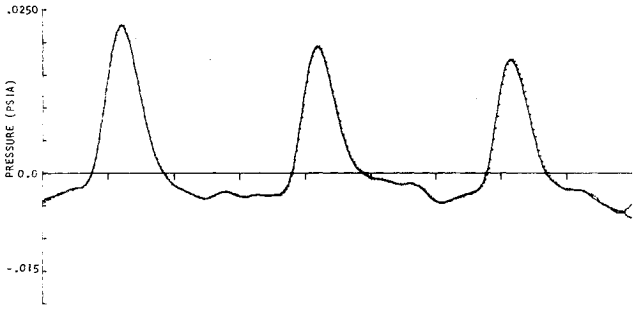

Fig. 4 Example of three rotor blade passage averaged trailing edge pressure transducer.

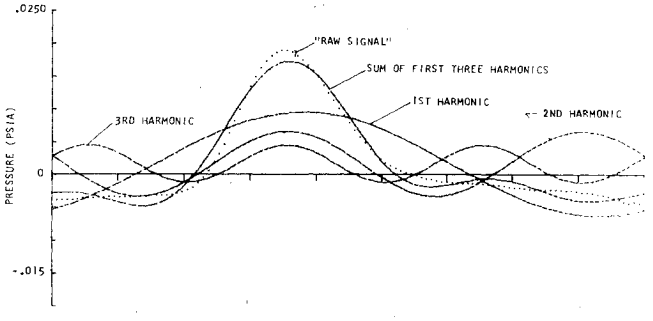

Fig. 5 Example of blade passage averaged signal and the first three harmonics for the trailing edge pressure transducer signal.

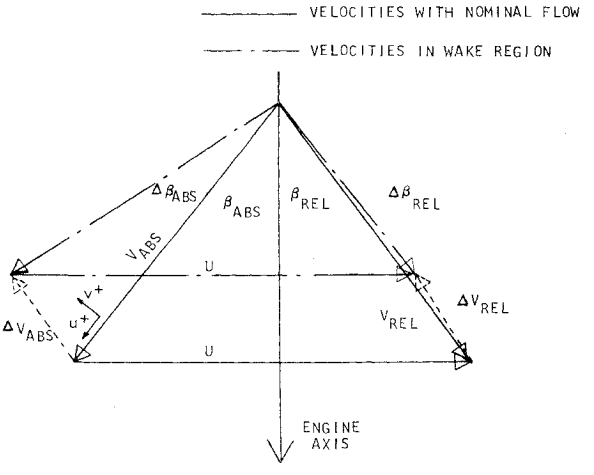

Fig. 6 Variation in rotor relative exit velocity creates corresponding velocity and angular change in absolute frame.

and pressure surfaces. From this, the times at which the wake was present at various locations were determined. The time increments between occurrences at the hot wire and the vane leading edge plane were then related to phase differences between the perturbation velocities and the vane surface. To simplify the experiment-theory correlation process, the data were adjusted in phase such that the transverse perturbation was at zero deg at the vane suction surface leading edge.

Following this procedure the pressure differences across a single vane at each transducer location were calculated. These difference data, along with the individual surface pressure data, were normalized with respect to an inlet flow parameter ($C_p = \Delta P/\rho \cdot V^2 \cdot v/V$, $C_p^* = P/\rho \cdot V^2 \cdot v/V$) where ρ is the inlet air density, V the stator inlet absolute velocity, and v the transverse perturbation velocity measured by the cross-wire probe.

Thus, the final form of the trailing edge unsteady pressure data described the time-variant pressure differential and is presented in terms of an aerodynamic phase lag referenced to a transverse gust at the airfoil leading edge, and a dynamic pressure coefficient C_p. It should be noted that there is always an arbitrary ± 360 deg $\cdot N$ inherent in the determination of the phase angle, i.e., a lag of 90 deg is equivalent to a lead of 270 deg.

These trailing edge unsteady pressure differential data are correlated with predictions obtained from the zero incidence, flat plate cascade and isolated flat plate airfoil, compressible transverse gust analysis of Ref. 4. The basic assumptions in this analysis are: the fluid is a perfect gas, the flowfield is irrotational, the thin airfoil approximations are appropriate, and the Kutta condition is valid at the trailing edge. It should be noted that although the axial velocity is relatively low, being on the order of 30.5 m/s, compressibility still plays an important role. This is because the compressible reduced frequency parameter $kM/\sqrt{1-M^2}$ is on the order of 0.8 which is well within the range wherein compressibility effects become significant. Hence, the compressible prediction $M=0.1$ is used for the correlation of the data.

Results

In this experimental investigation, a qualitative study of the rotor wake together with the quantitative investigation of the resulting time-variant surface pressures induced in the trailing edge region of the stator vanes was undertaken.

The velocity is the fundamental quantity used to define the wake and was measured with the cross-wire probe as previously described. This measurement, made in the absolute or non-rotating reference frame, together with the absolute flow angle and rotor speed were used to calculate the velocities in the relative or rotating frame of reference. It should be noted that although the rotor wakes are the forcing function for the time-variant pressure on the stator vanes, all of the data were decomposed and harmonically analyzed. As a result, only the magnitude of each harmonic of the fluctuating transverse velocity in the wake which induces the corresponding unsteady pressure on the downstream vane enters into the data analysis. In particular, the wake data determine the value of v for each harmonic which is used to calculate the nondimensionalizing factor $\rho \cdot V^2 \cdot v/V$ for C_p and C_p^*, as previously noted.

Figure 7 demonstrates the variation in the wake profile with axial distance as measured from the rotor trailing edge for two values of loading (compressor pressure ratio) along the 100% speed line. At a constant axial distance from the rotor, an increase in the pressure ratio (a decrease in the mass flow rate) can be seen to result in an increase in both the width and velocity deficit of the wake. As the axial distance from the rotor is increased, the wake decays and the difference between the wake centerline velocity and the freestream velocity decreases. At the high level of loading this trend is very pronounced but is much less significant at the lower level of loading. The trailing edge region pressure differential data for 0, ± 5, and ± 10 deg of incidence at a reduced frequency of 7.5 together with the slightly compressible $M=0.1$ zero incidence predictions for the isolated classical flat plate are presented in Fig. 8. This incidence variation was accomplished by rotating the isolated vane.

As indicated, the aerodynamic phase lag data generally correlate well with the predictions, with the -10 deg incidence angle case exhibiting the poorest correlation. Of greater interest are the dynamic pressure coefficient data for this isolated flat plate. These dynamic pressure coefficient data are seen to be increased in value as compared to the predictions for all values of the incidence angle, with the zero incidence data exhibiting the best correlation. The discrepancy between the dynamic pressure coefficient data and the predictions increases with the absolute value of the incidence angle. However, the trend exhibited by all of these isolated airfoil dynamic pressure data clearly indicates that the pressure differential at the trailing edge (100% chord) would attain a value of zero, i.e., the Kutta condition appears to be satisfied for all incidence angles for the classical isolated flat plate at high reduced frequency.

Figure 9 presents the classical flat plate stator row trailing edge data for 0, -2, and $-6\frac{1}{2}$ deg of incidence together with the corresponding slightly compressible $M=0.1$ zero incidence flat plate cascade predictions. The reduced frequency for these flat plate cascade data ranges from 7.3 to 8.4. It should be noted that in this case the incidence angle variation was achieved by loading the compressor along a constant

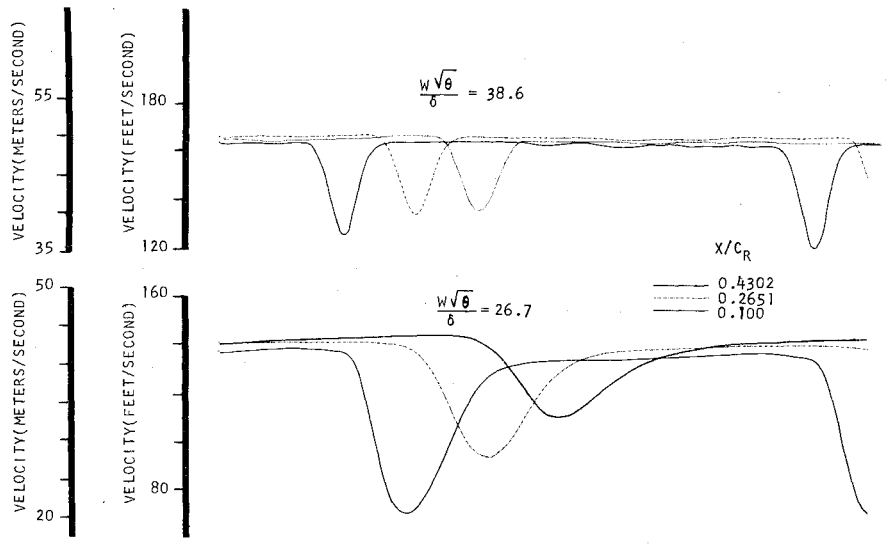

Fig. 7 Variation of the rotor wake profile with axial distance for two levels of loading.

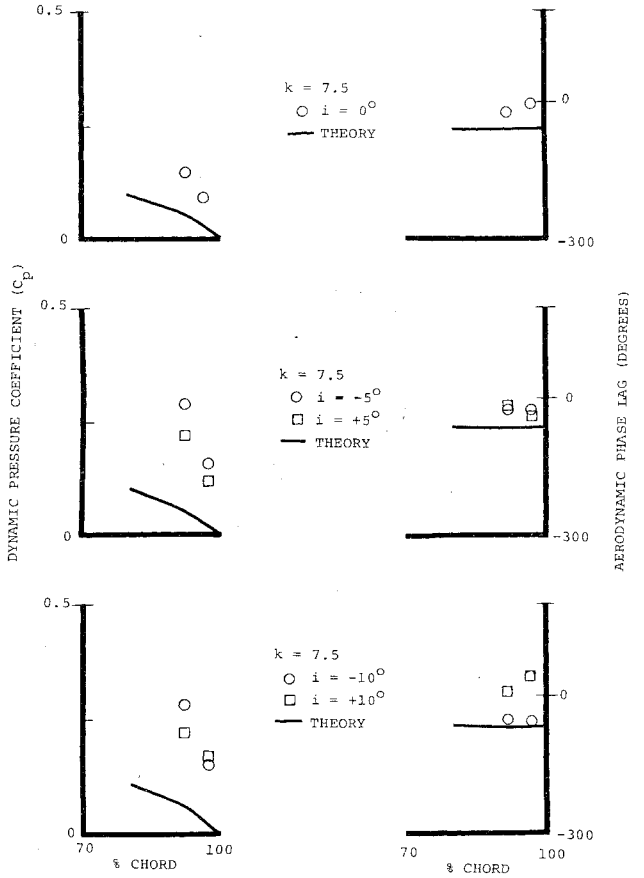

Fig. 8 Trailing edge region unsteady pressure differential variation for the isolated flat plate.

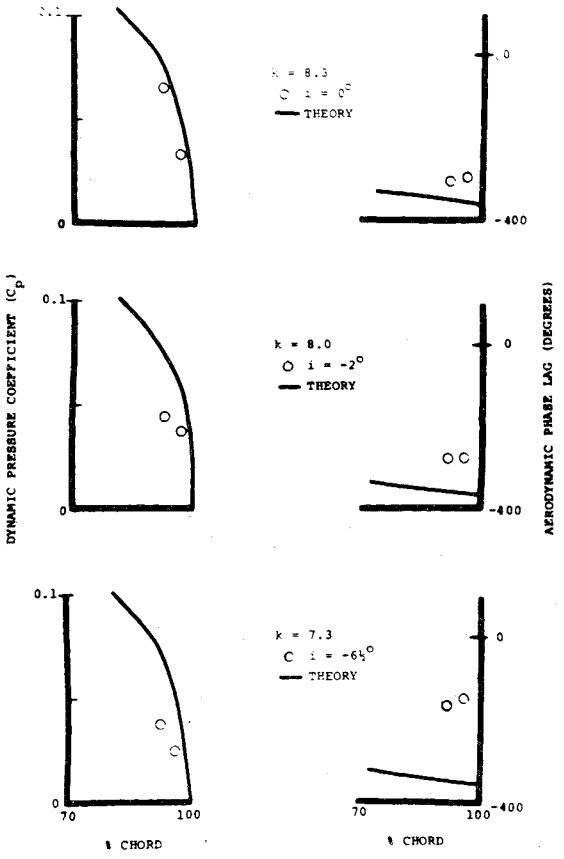

Fig. 9 Trailing edge region unsteady pressure differential variation for the flat plate cascade.

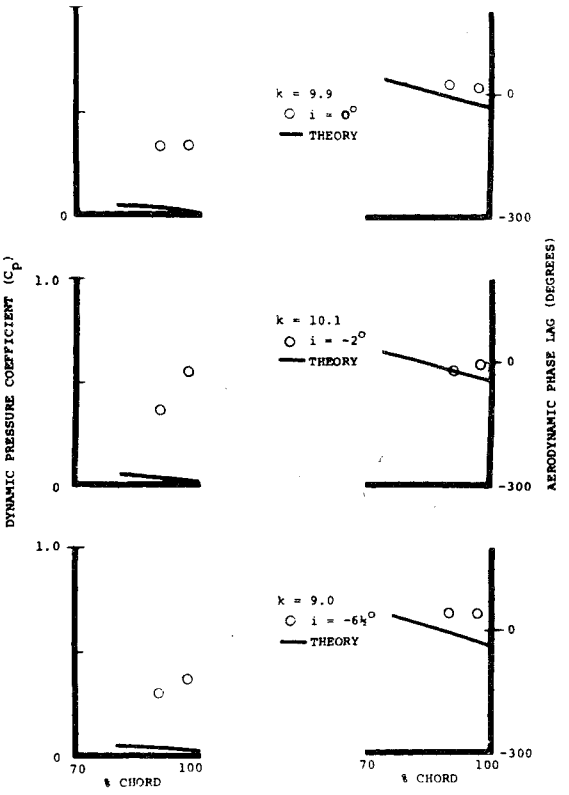

Fig. 10 Trailing edge region unsteady pressure differential variation for the cambered airfoil cascade.

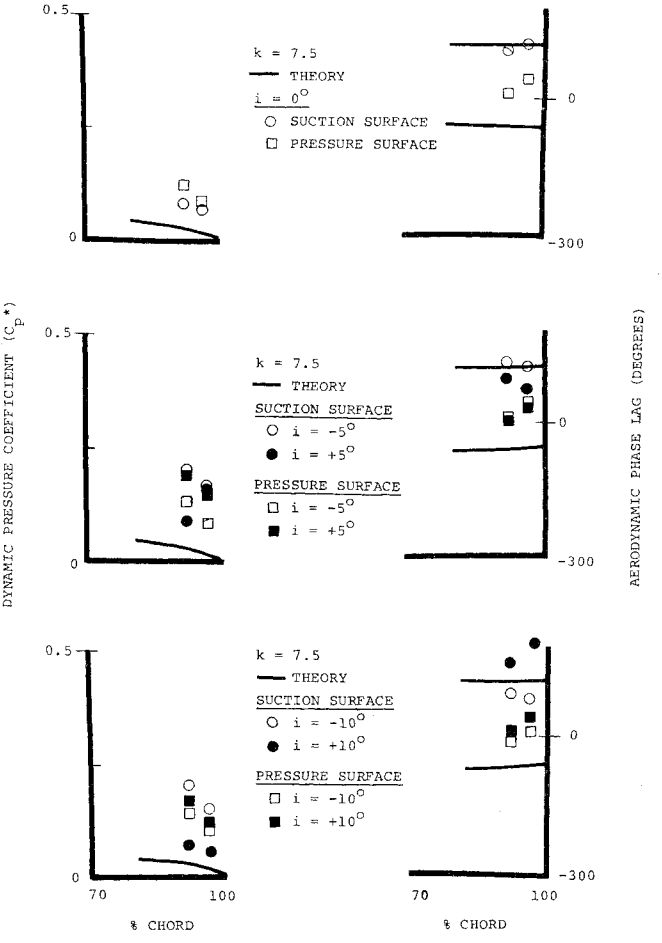

Fig. 11 Trailing edge region unsteady surface pressure variations for the isolated flat plate.

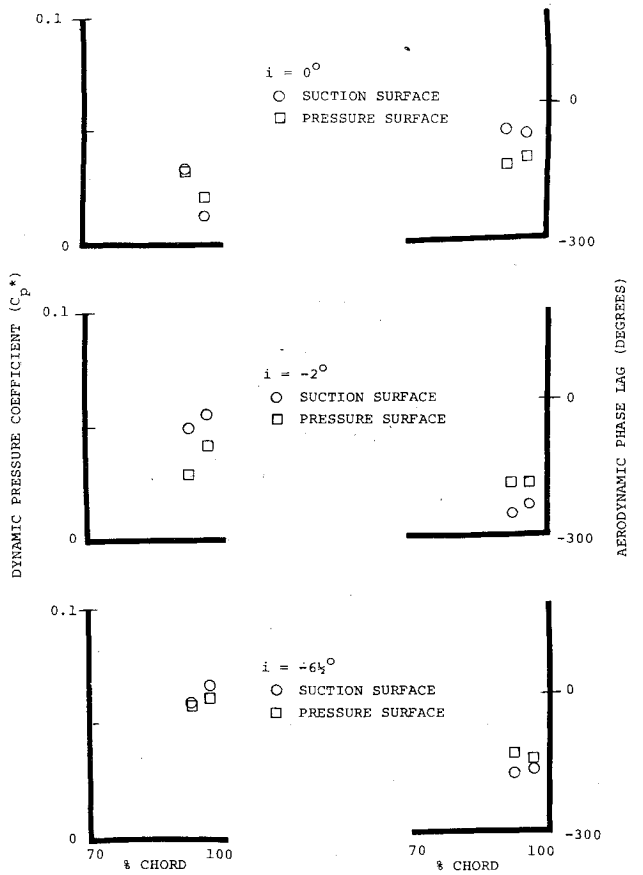

Fig. 12 Trailing edge region unsteady surface pressure variations for the flat plate cascade.

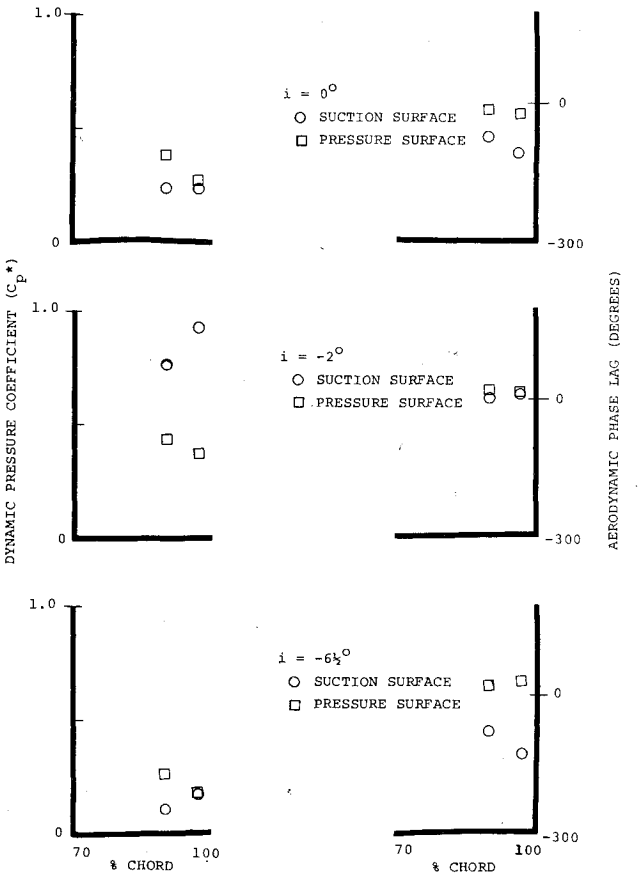

Fig. 13 Trailing edge region unsteady surface pressure variations for the cambered airfoil cascade.

speed line and that no indications of stalling, such as a loss in performance, were noted until much larger incidence values.

The zero incidence angle flat plate cascade aerodynamic phase lag data exhibit reasonably good correlation with the prediction. As the incidence angle is decreased from zero, however, the phase lag data increase in value and the correlation becomes less satisfactory.

The dynamic pressure coefficient data are seen to be decreased in value as compared to the predictions, in contrast to the previously discussed isolated airfoil data. The zero incidence angle data correlate quite well with the prediction; the discrepancy between the data and the prediction increasing as the incidence angle decreases from zero. However, as with the isolated flat plate, the trend of all of these dynamic pressure coefficient data indicates that at the trailing edge (100% chord) of the cascaded flat plate airfoil, the pressure differential will be zero. Thus, for the classical flat plate cascade as well as the classical isolated flat plate, it appears that the Kutta condition is satisfied over a wide range of incidence angle values at high reduced frequency.

The trailing edge region time-variant pressure data for the cambered airfoil stator row and the corresponding flat plate predictions are presented in Fig. 10. The incidence angle values are 0, -2, and $-6\frac{1}{2}$ deg with the reduced frequency ranging from 9.0 to 10.1. As for the flat plate stator row, this incidence angle variation was achieved by loading the compressor along a constant speed line and no indications of stall, such as a loss in performance, were noted at these incidence values.

The correlation of the cambered airfoil cascade aerodynamic phase lag data with the flat plate cascade prediction is good for all incidence angle values.

The dynamic pressure coefficient data are seen to be significantly increased over the predictions for all values of the incidence angle. In fact, the magnitude of these cambered cascade dynamic pressure coefficient data are noticeably larger than the corresponding flat plate data previously discussed. In contrast to the classical isolated flat plate and flat plate cascade results, these cambered airfoil cascade trailing edge data give no indication that the value of the pressure differential at the trailing edge is approaching zero, in fact, the trend of the -2 and $-6\frac{1}{2}$ deg data indicate an increased value at the trailing edge. Hence, it appears that the Kutta condition is not satisfied for the cambered airfoil cascade at high reduced frequency values.

To gain some insight into the fundamental differences between the classical flat plate and cambered airfoil cascade results, the individual pressure and suction surface trailing edge region unsteady data for the isolated flat plate, the flat plate cascade, and the cambered airfoil cascade are presented in Figs. 11, 12, and 13, respectively.

Figures 11 and 12 demonstrate that for the cases wherein the Kutta condition is satisfied, i.e., the classical isolated flat plate and flat plate cascade, the pressure and suction surface dynamic pressure coefficient data $C_p^* = P/\rho \cdot V^2 \cdot v/V$ vary at approximately the same rate in this trailing edge region. The differences between the pressure and suction surface aerodynamic phase lag data for these cases either remain constant or, in a limited number of cases, decrease.

The pressure and suction surface time-variant pressure data for the cambered airfoil cascade on which the Kutta-Joukowsky condition was not satisfied are presented in Fig. 13. In contrast to the previously discussed classical flat plate cases, these pressure and suction surface dynamic pressure coefficient data do not change at the same rate. Also, the differences between the pressure and suction surface phase lag data either remain constant, as per the flat plate cases, or increase.

Summary and Conclusions

The time-variant pressure distribution in the trailing edge region of a classical isolated flat plate, a classical flat plate

cascade, and a cambered airfoil cascade were measured over a range of incidence angles at high reduced frequency values. These pressure and suction surface data were analyzed to determine the complex fluctuating surface pressure and pressure differential and the latter correlated with appropriate zero incidence, compressible, flat plate predictions. These results indicate the following:

1) The Kutta-Joukowsky condition appears to be satisfied on the classical isolated flat plate and flat plate cascade at high reduced frequency values for all of the incidence angles investigated.

2) The Kutta-Joukowsky condition does not appear to be satisfied by the cambered airfoil cascade at these high reduced frequency values.

3) The pressure and suction surface dynamic pressure coefficient data vary at approximately the same rate in the chordwise direction in the trailing edge region of the isolated flat plate and the flat plate cascade, but at different rates for the cambered airfoil cascade.

4) The difference between the pressure and suction surface aerodynamic phase lag data either remains constant or decreases as the trailing edge is approached for the isolated flat plate and the flat plate cascade but increases or remains constant for the cambered airfoil cascade.

Acknowledgment

This research was sponsored in part by the Air Force Office of Scientific Research. Acknowledgment is made to General Motors for permission to include the flat plate data.

References

[1] Sears, W.R., "Unsteady Motion of Airfoils with Boundary Layer Separation," *AIAA Journal*, Vol. 14, Feb. 1976, pp. 216-220.

[2] McCroskey, W.J., "Some Current Research in Unsteady Fluid Dynamics," *Journal of Fluids Engineering*, Vol. 99, March 1977, pp. 8-30.

[3] Sears, W.R., "Some Aspects of Nonstationary Airfoil Theory and its Practical Application," *Journal of the Aeronautical Sciences*, Vol. 8, Jan. 1941, pp. 104-108.

[4] Fleeter, S., "Fluctuating Lift and Moment Calculations for Cascaded Airfoils in a Nonuniform Compressible Flow," *Journal of Aircraft*, Vol. 10, Feb. 1973, pp. 93-98.

[5] Satyanarayana, B. and Davis, S., "Experimental Studies of Unsteady Trailing Edge Conditions," *AIAA Journal*, Vol. 16, Feb. 1978, pp. 125-129.

[6] Commerford, G.L. and Carta, F.O., "Unsteady Aerodynamic Response of a Two-Dimensional Airfoil at High Reduced Frequency," *AIAA Journal*, Vol. 12, Jan. 1974, pp. 43-48.

[7] Archibald, F.S., "Unsteady Kutta Condition at High Values of the Reduced Frequency Parameter," *Journal of Aircraft*, Vol. 12, June 1975. pp. 545-550.

[8] Ostdiek, F.R., "A Cascade in Unsteady Flow," *Unsteady Phenomena in Turbomachinery*, AGARD CP 177, Sept. 1975.